ACS Sustainable Chemistry & Engineering

pubs.acs.org/journal/ascecg

Research Article

Highly Reduced Graphene Assembly Film as Current Collector for Lithium Ion Batteries

Yuwei Zhao,[⊥] Jinlong Yang,[⊥] Jingjing Ma, Qian Wu, Wei Qian, Zhe Wang, Haining Zhang, Daping He,* and Shichun Mu*

Cite This: *ACS Sustainable Chem. Eng.* 2021, 9, 8635–8641

Read Online

ACCESS | Metrics & More | Article Recommendations | Supporting Information

ABSTRACT: With the development of lithium ion batteries (LIBs), further increasing the energy densities of batteries is urgent. Graphene, with excellent chemical stability, high conductivity, and light weight, is an ideal material to improve the battery energy density by replacing traditional metal current collectors. Accordingly, we report a large-size (120 mm × 120 mm) graphene assembled film (GAF) with high crystallinity, electrical conductivity ($(2.30 \pm 0.06) \times 10^5$ S m^{-1}) and ultralight weight (3.18 mg cm^{-2}). The electrode/GAF interface has better wetting and lower contact resistance. When all the metal (Al/Cu) current collectors are replaced by GAF, the energy density of the full cell electrode can increase by 32.9% (with an areal density of 4 mAh cm^{-2}). Moreover, the electrode with GAF current collectors shows improvements in cycling stability, rate capability, and capacity. Undoubtedly, these results suggest that GAF has broad prospects as a high-energy-density lithium ion current collector.

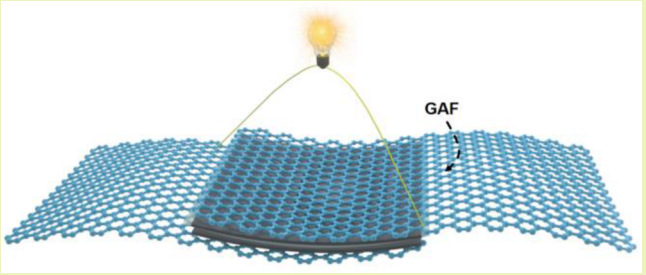

KEYWORDS: *Graphene film, Reduced graphene, Lightweight, High temperature reduction, Current collector, Lithium ion batteries, High energy density*

INTRODUCTION

With the rapid development of portable electronic equipment, lithium ion batteries (LIBs) with high energy density and long cycle life are urgently needed.[1,2] Thus, a large number of high-capacity electrode materials have been developed.[3−5] However, little research has been conducted on lightweight current collectors.[6−8] In fact, the current collector can play an important role in the energy efficiency, rate performance, and cycle stability of an LIB.[9] The current collector materials of commercial LIBs are mainly metal materials, such as copper (Cu) foil and aluminum (Al) foil. However, such metal current collectors do not contribute to the capacity of the battery, and the large mass of a metal current collector makes the battery lose an amount of energy density and flexibility.[10] Moreover, the adhesion ability of a metal current collector to the electrode material is usually weak, leading to a volume expansion effect during the charge and discharge processes and decreasing performance at a high rate.[11] To solve such problems, structures of metal current collectors with roughened surfaces, such as nanoporous, nanoneedles, and nanonetworks, have been designed.[11−13] However, the high-quality density of the metal itself still limits the increase in the energy density of the battery. More importantly, metal foil is susceptible to local corrosion during long-term cycles, which reduces the service life of the battery.

To improve the energy density and solve the corrosion problem of the metal current collector, finding a new lightweight and corrosion-resistant material is urgently necessary. Due to their good properties, carbon materials are favored by many researchers.[14] Among them, graphene is a promising current collector material because of its high conductivity, excellent chemical stability, and light weight.[15−20] As reported, graphene has been used to modify the surface of metal foil. For example, Wang et al. used plasma-enhanced chemical vapor deposition to directly grow graphene on the surface of Al foil as a conductive and interface barrier layer.[21] Kim et al. prepared a graphene film by chemical vapor deposition and transferred it to the surface of an Al foil by a roll to roll transfer method to improve the corrosion resistance and energy density of the current collector.[22] However, due to the presence of the metal foil, the current collector still has a risk of corrosion. More importantly, these metal current collectors still have a high proportion of mass, which limits the energy density of the battery. Chen et al. prepared graphene films by Joule heating and used them as current collectors for LIBs.[23] However, the size of the graphene films obtained by Joule heating was too small to be widely used. Therefore, it is

Received: April 8, 2021
Revised: June 7, 2021
Published: June 16, 2021

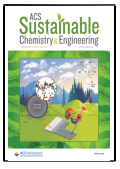

https://doi.org/10.1021/acssuschemeng.1c02414
ACS Sustainable Chem. Eng. 2021, 9, 8635–8641

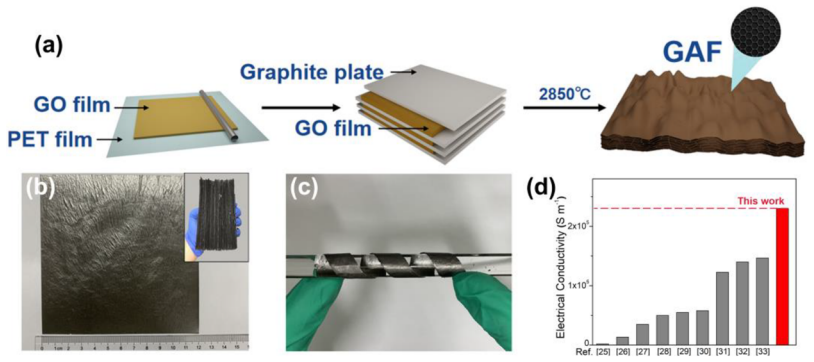

Figure 1. (a) Schematic of GAF fabrication procedure. (b) A 120 mm × 120 mm GAF sample reduced by the high-temperature process. Inset: 100 GAFs are produced in a high temperature reduction process at one time. (c) GAF is bent around a glass rod. (d) Comparison of electronic conductivities between GAF and reported graphene films.

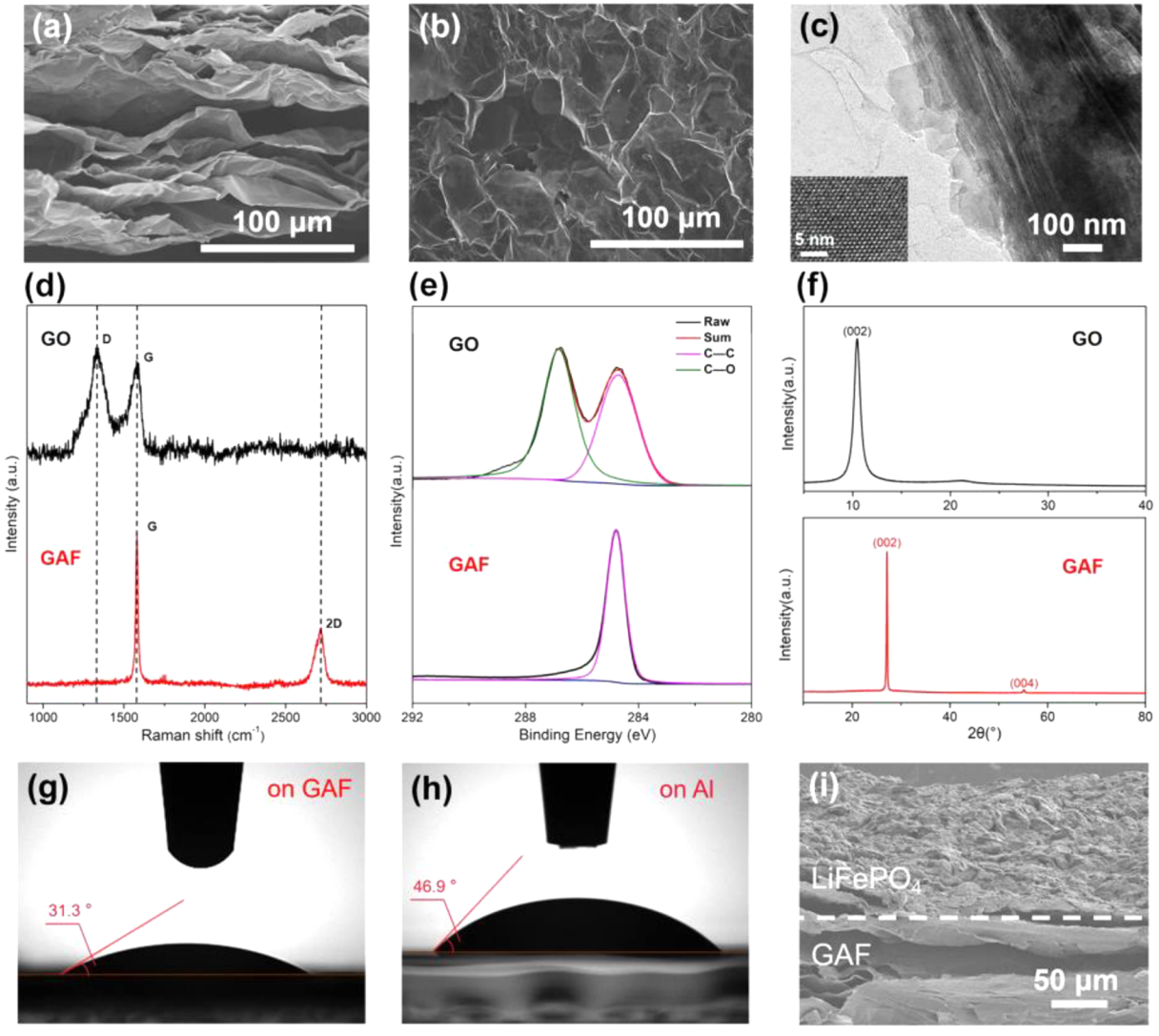

Figure 2. (a) Cross-sectional SEM images of GAF. (b) Surface morphology of GAF. (c) TEM image of exfoliated GAF. Inset: partially enlarged image. (d) Raman, (e) XPS, and (f) XRD pattern comparisons of unannealed GO film and GAF. (g, h) Contact angles of $LiFePO_4$ slurry dropping (g) on GAF and (h) on Al foil. (i) Cross-sectional SEM image of $LiFePO_4$ cathode coated on GAF after drying.

significant to develop a new method for the large-scale production of graphene current collectors with light weight, high conductivity, and practical application value for the new generation of high energy density LIBs.

Here, we develop a highly conductive layered graphene assembled film (GAF), which can completely replace metal foil as a LIB current collector and significantly increase the energy density of the electrode. The size of the GAF obtained by high temperature annealing reaches 120 mm × 120 mm, and the

https://doi.org/10.1021/acssuschemeng.1c02414
ACS Sustainable Chem. Eng. 2021, 9, 8635−8641

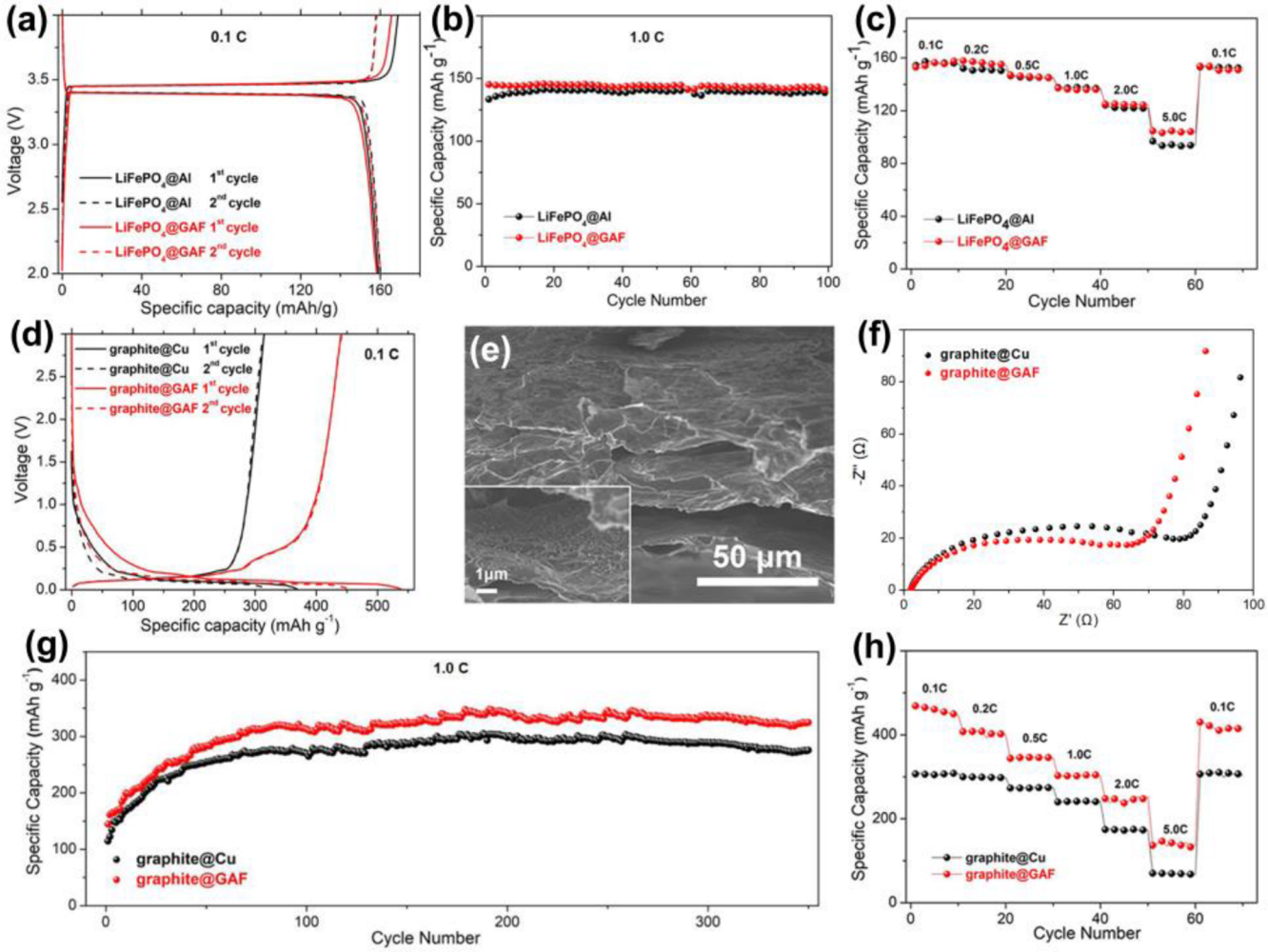

Figure 3. (a) Charge−discharge curves of initial two cycles. (b) Cycling performances and (c) rate performances of $LiFePO_4$/GAF and $LiFePO_4$/Al electrodes. (d) Charge−discharge curves of initial two cycles of graphite/GAF and graphite/Cu electrodes. (e) SEM images of graphite/GAF electrodes after 20 cycles. (f) EIS of graphite anode on different current collectors. (g) Cycling and (h) rate performances of graphite/GAF and graphite/Cu electrodes.

film can be mass-produced. The areal density of GAF is only 3.18 mg cm^{-2}, which is much lower than that of commercial metal foil. Moreover, GAF has high conductivity ($(2.3 \pm 0.1) \times 10^5$ S m^{-1}), and the rough surface of GAF assembled from graphene sheets makes the slurry easier to penetrate, leading to better wettability. When GAF is used as both cathode and anode current collectors, the assembled battery shows significantly improved energy density and higher rate performance and cycle stability than that with Al/Cu foil collectors.

EXPERIMENTAL SECTION

Fabrication of GAF. Dispersed graphene oxide with a solid content of 3% was put in ultrapure water and converted into a gel. The produced gel was coated to form a film and dried. Then the graphene oxide (GO) film was stacked vertically and separated by a graphite plate in the middle for batch production. The GO film was placed in a high-temperature furnace with an argon atmosphere and heated at 1300 °C for 2 h and at 2850 °C for 1 h. Finally, slow cooling to room temperature was performed to obtain GAF.

Fabrication of Electrodes with GAF and Metal Current Collectors. Electrode slurry was made by mixing commercial lithium iron phosphate ($LiFePO_4$, LFP) or commercial graphite, carbon black, and polyvinylidene fluoride (PVDF) in *N*-methyl-2-pyrrolidone (NMP) at a ratio of 8:1:1. The slurry was coated smoothly on GAF, aluminum foil, and copper foil, respectively. Then the coated film was dried at 100 °C for 10 h. When cooled to room temperature, electrodes with GAF and metal current collectors were obtained.

RESULTS AND DISCUSSION

The GAF preparation process is shown in Figure 1a. First, GO is dispersed in ultrapure water and mechanically stirred into a GO gel. Then the GO gel is coated with a scraper onto a PET board to form a film. After drying, GO is reduced at 2850 °C in an argon atmosphere to obtain GAF with a large size of 120 mm × 120 mm. In battery production, the size and flexibility of the electrodes are very important, because they are required in processing steps such as coating, rolling, and folding.[24] In this work, GAF has a larger size and can be mass-produced (Figure 1b) with good flexibility (Figure 1c), indicating our method is suitable for practical applications. The areal density of GAF (3.18 mg cm^{-2}) is only 58% that of Al foil and 36% that of Cu foil (Figures S1−S3), which greatly increases the mass ratio of active materials in the electrode. The conductivity of GAF ($(2.3 \pm 0.1) \times 10^5$ S m^{-1}) is further compared with those of previously reported graphene films (Figure 1d).[25−33] The results show that the conductivity of large-size GAF is higher than those of most reports. The high conductivity makes it

https://doi.org/10.1021/acssuschemeng.1c02414
ACS Sustainable Chem. Eng. 2021, 9, 8635−8641

possible for the current collector of an LIB to obtain a high electrochemical performance.

Figure 2a shows the layered structure of GAF, which minimizes the internal stress after folding, allowing GAF to have good flexibility. Furthermore, it can be seen that GAF has a very rough surface (Figure 2b), which is beneficial to improving the bonding force of interfaces between GAF and the active material. In addition, during the charging and discharging process, part of the electrolyte can enter the layered structure through pores on the GAF surface to contribute a part of the battery capacity. A high-resolution transmission electron microscopy (HRTEM) image further shows the reduced GO sheets and the sp^2 structure of GAF, proving that GAF is assembled with highly graphitized graphene (Figure 2c, Figure S4). By contrast, the TEM image of the graphene sheet assembled into GO film is shown in Figure S5.

Raman spectroscopy shows that GO has a significant D peak (1350 cm^{-1}) related to defective carbon (Figure 2d). After reduction at high temperatures, the D peak almost disappears, while the high-intensity G peak (1600 cm^{-1}) related to crystalline carbon occurs, indicating the high crystallinity of GAF. By comparison with recent reports, this shows that GAF has an higher degree of reduction (Table S1). Moreover, a clear 2D peak can be noticed at 2700 cm^{-1} of the GAF spectrum, proving the existence of the graphene layer.[24] The XPS spectrum (Figure 2e) shows a strong C−O peak at 286.8 eV for GO; after reduction at high temperatures, this peak is almost undetectable, confirming the near removal of oxygen-containing groups in GAF. The C−C peak intensity of GAF at 284.5 eV is high and sharp, proving the high degree of graphitization of GAF, which allows GAF to have good conductivity. The XRD pattern (Figure 2f) only reveals a strong peak (002) at 2θ = 26.61°, also indicating the highly graphitized graphene for GAF and a decreasing interlayer distance (d = 0.335 nm) compared with GO (d = 0.846 nm). This evidences that some oxygen-containing groups were removed during the high-temperature reduction procedure, which is consistent with the XPS analysis.

The wetting properties of the interfaces of lithium iron phosphate ($LiFePO_4$, LFP)/GAF and $LiFePO_4$/Al were investigated. As shown in Figure 2g,h, the contact angle (31.3°) of $LiFePO_4$ on the GAF surface is much smaller than that on the Al surface (46.9°), indicating that the surface tension of the $LiFePO_4$/GAF interface is relatively small. Such good wettability indicates the stronger adhesion of the $LiFePO_4$/GAF interface than that of the $LiFePO_4$/Al interface. We further measured the adhesion between GAF and $LiFePO_4$ through a shear test (Figure S6), and the results show once again that GAF has stronger adhesion to $LiFePO_4$ than Al does. As shown in Figure S7, after drying, the coated $LiFePO_4$ layer on Al foil shrinks in some areas while it does not shrink when applied to GAF, which further proves the strong adhesion of the lithium iron phosphate/GAF interface. Figure 2i demonstrates that the active material forms a fine contact with GAF, which provides a good way for the electron transmission between the active material and the current collector. For a more comprehensive explanation, the SEM image of graphite coated on GAF is shown in Figure S8.

To investigate the influence of the GAF current collector on the electrochemical performance of LIBs, a half-cell was first assembled with lithium metal as the anode and $LiFePO_4$/GAF as the cathode. As a reference, a half-cell with commercial $LiFePO_4$ coated Al foil was assembled simultaneously. From the charge−discharge curve of the initial two cycles under 0.1 C (1.0 C = 170 mA g^{-1}) current density (Figure 3a), it can be seen that the first discharge capacity of the $LiFePO_4$/GAF battery is about 158 mAh g^{-1}, similar to that of the $LiFePO_4$/Al battery. The first Coulombic efficiency of the $LiFePO_4$/GAF battery is 95.0%, higher than that of the $LiFePO_4$/Al battery (93.82%). We believe that this is because the rough surface of GAF provides a larger contact area with the active material and reduces the internal contact resistance. Figure 3b shows the 100-cycle performance of the battery at a current density of 1.0 C. The specific capacity of the $LiFePO_4$/GAF battery is stable at 143.2 mAh g^{-1}, which is very similar to the specific capacity of the $LiFePO_4$/Al battery at 139.6 mAh g^{-1}. The energy densities of the two battery cathodes are shown in Figure S9. When calculating with the total mass of the active material and the current collector, GAF has a significant effect on improving the energy density of the electrode. We further tested the rate performance of the battery at a current density of 0.1−5.0 C (Figure 3c). When the current density is between 0.1 and 1.0 C, the two batteries have similar specific capacities. As the current density continues to increase, the $LiFePO_4$/GAF battery gradually exhibits a higher specific capacity than the $LiFePO_4$/Al battery. When the current density further reaches 5.0 C, the specific capacity of the $LiFePO_4$/GAF battery is 104.67 mAh g^{-1}, which is 11.1% higher than that (94.22 mAh g^{-1}) of the $LiFePO_4$/Al battery. Interestingly, when the current density is reduced to 0.1 C again, the specific capacity of the $LiFePO_4$/GAF battery can also be completely restored, proving the good cycling stability of GAF under high current densities. Electrochemical impedance spectroscopy (EIS) analysis presents that the kinetics of lithium ion transport is faster in the $LiFePO_4$/GAF battery than in the $LiFePO_4$/Al battery (Figures S10 and S11).[34] At least two reasons can account for this: First, the surface of GAF is much rougher than that of Al foil, which makes the contact between GAF and the active material closer. Second, GAF and conductive carbon black have the same work function, while Al foil and conductive carbon black have different work functions in the cell, which allows electrons to pass through the interface between GAF and the active material more smoothly.[35,36]

We further explored the impact of GAF as an anode current collector on battery performance. Commercial graphite was used as the anode material to assemble half-cells with lithium metal||graphite/GAF. As a comparison, lithium metal||-graphite/Cu half-cells were fabricated simultaneously. The first two cycles of charge and discharge curves at 0.1 C (1.0 C = 372 mA g^{-1}) reveal the excellent specific capacity of the graphite/GAF battery (Figure 3d). The first cycle discharge specific capacity reaches 538.0 mAh g^{-1}, which is significantly higher than that of the graphite/Cu battery (368.1 mAh g^{-1}). This is because part of GAF is involved in the deintercalation of lithium ions. In the low voltage region of 0−0.25 V, the graphite region is first intercalated with lithium ions. In this region, the curves of the two batteries are similar. In the voltage range 0.25−1.0 V, the GAF partially begins to be embedded with lithium ions, and an obvious turning point occurs in the curve of the graphite/GAF battery. The specific capacity continually rises, finally obtaining a capacity increase of 169.9 mAh g^{-1}. To verify this point of view, an empty GAF film without active materials as the anode was employed to assemble the half-cell. The measured capacity is 0.4 mAh cm^{-2}

https://doi.org/10.1021/acssuschemeng.1c02414
ACS Sustainable Chem. Eng. 2021, 9, 8635−8641

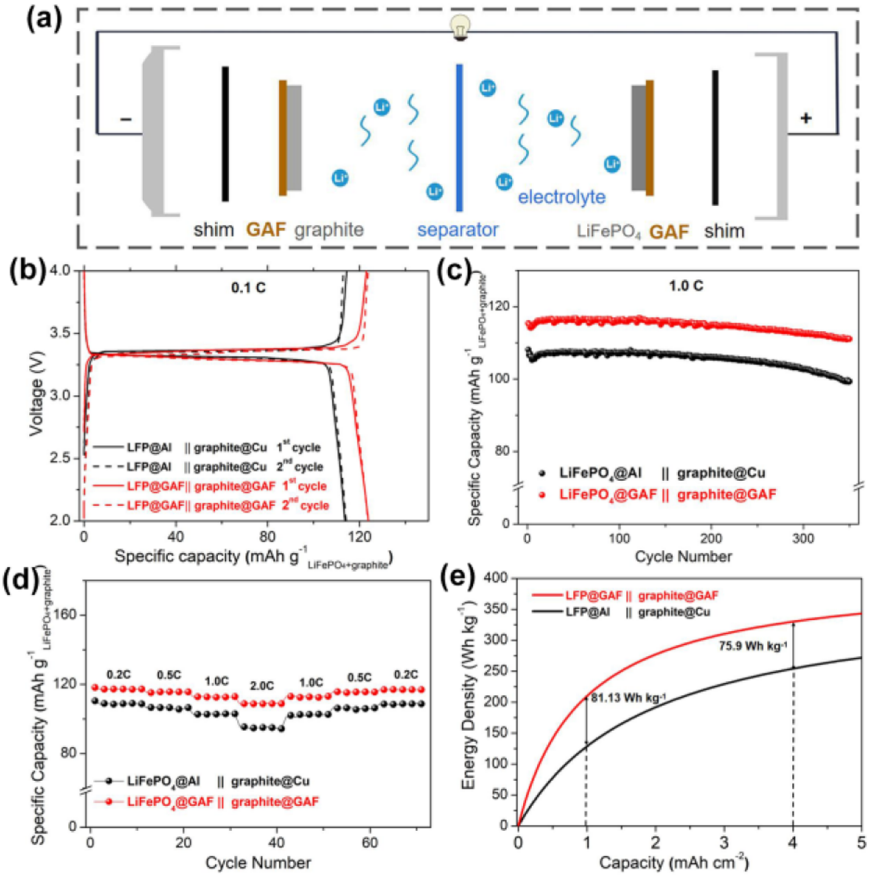

Figure 4. (a) Structure diagram of GAF current collector full cell. (b) Charge−discharge curves of initial two cycles at 0.1 C of two full cells. (c) Cycling performances of two full cells. (d) Rate performances of two full cells. (e) Comparison of energy densities of two full cell electrodes.

(Figure S12), which evidences that GAF can provide part of the capacity for the electrode during charge and discharge. The cross-sectional SEM image of the GAF after 20 cycles exhibits no structural damage to the GAF after the cycles (Figure 3e). As expected, part of the lithium deposition between the GAF layers can be observed. Moreover, the multilayer structure of GAF can adjust the volume expansion of the negative electrode material during the charge and discharge process to a certain extent, thereby improving the overall cycle performance of the battery.[37] The EIS results of the two batteries also demonstrate that the kinetics of lithium ion transmission in the graphite/GAF battery is faster (Figure 3f).

Next, the performance of the battery for 350 cycles at a current density of 1.0 C (Figure 3g) was tested. At the beginning of the cycle, the specific capacity of the battery continues to increase, which represents an electrochemical activation process of the battery. After 75 cycles, the capacity of the graphite/GAF battery is 313 mAh g^{-1}, and the increasing trend becomes gentle, while it is 271 mAh g^{-1} for the graphite/Cu battery. After 350 cycles, the specific capacity of the graphite/GAF battery is still maintained at 324 mAh g^{-1}, while it is 275 mAh g^{-1} for the graphite/Cu battery. Figure 3h shows the comparison of the rate performances of the two batteries. Under different current densities, the graphite/GAF battery always has a significant increase in specific capacity, even at a large current density. At a current density of 5.0 C, the specific capacity of the graphite/Cu battery drops to 69 mAh g^{-1}, while the graphite/GAF battery maintains a specific capacity of 141 mAh g^{-1} and can recover the capacity when the current decreases. These results indicate that GAF can increase the capacity of the anode in an LIB and has great cycle stability and rate performance.

To verify the actual application value of GAF, full cells were fabricated, with $LiFePO_4$ as the cathode active material, graphite as the anode active material, and GAF as the current collectors (GAF battery) (Figure 4a) compared to full cells with an Al foil current collector for the cathode and an Cu foil current collector for the anode (metal foil battery). The first two cycle charge−discharge curves of the two batteries are shown in Figure 4b. When the sum of the active material masses of cathode and anode is calculated, the initial specific capacity of GAF battery is 123.6 mAh g^{-1}, while it is 114.1 mAh g^{-1} for the battery with the metal current collectors. At a current density of 1.0 C (1.0 C = 170 mA g^{-1}), the specific capacity of the GAF battery after 350 cycles is 111.04 mAh g^{-1}. The capacity holding ratio is 95.42%, while that of the metal foil battery is 92.52% (Figure 4c). Figure 4d exhibits the rate performance comparison of the two batteries. As the current density gradually increases, the specific capacity of the GAF battery shows an obvious increase. At a current density of 2.0 C, it has a specific capacity of 108.7 mAh g^{-1}, which is higher than that of the metal foil battery (94.8 mAh g^{-1}). These results demonstrate that GAF has a improved effect on the cycling and rate performance of an LIB.

Last, we evaluated the influence of GAF on the energy density of an LIB (Figure 4e). Considering the total mass of active materials and current collectors, as the surface capacity of the electrode is 1 mAh cm^{-1}, the energy density of

https://doi.org/10.1021/acssuschemeng.1c02414
ACS Sustainable Chem. Eng. 2021, 9, 8635−8641

$LiFePO_4$/Al‖graphite/Cu electrode is 128.6 Wh kg^{-1}, while it reaches 209.8 Wh kg^{-1} for the $LiFePO_4$/GAF‖graphite/GAF full cell. As the surface capacity reaches the standard 4 mAh cm^{-1}, the energy density of $LiFePO_4$/Al‖graphite/Cu electrode is 254.1 Wh kg^{-1}, while it is 330.0 Wh kg^{-1} for the $LiFePO_4$/GAF‖graphite/GAF full cell, which is 32.9% higher than that of the former. This indicates the significant advantages of GAF for improving the energy density of LIBs.

CONCLUSION

In summary, we designed and constructed an advanced graphene assembly film (GAF) with high crystallinity, larger size (120 mm × 120 mm), high conductivity ($(2.30 \pm 0.1) \times 10^5$ S m^{-1}), and ultralightweight mass (3.18 mg cm^{-2}), which can be produced in batches. When replacing traditional metal current collectors to assemble half-cells and full cells, the capacity and the rate and cycle stability performances were all enhanced. Most importantly, GAF significantly increased by 32.9% the energy density of LIB electrodes. Undoubtedly, our work is a promising and feasible option to increase the electrochemical performance and energy density of LIBs.

ASSOCIATED CONTENT

Supporting Information

The Supporting Information is available free of charge at https://pubs.acs.org/doi/10.1021/acssuschemeng.1c02414.

Experimental details and additional characterization (PDF)

AUTHOR INFORMATION

Corresponding Authors

Shichun Mu − *State Key Laboratory of Advanced Technology for Materials Synthesis and Processing, Wuhan University of Technology, Wuhan 430070, China; Foshan Xianhu Laboratory of the Advanced Energy Science and Technology Guangdong Laboratory, Xianhu hydrogen Valley, Foshan 528200, China;* orcid.org/0000-0003-3902-0976; Email: msc@whut.edu.cn

Daping He − *Hubei Engineering Research Center of RF-Microwave Technology and Application, Wuhan University of Technology, Wuhan 430070, China;* orcid.org/0000-0002-0284-4990; Email: hedaping@whut.edu.cn

Authors

Yuwei Zhao − *State Key Laboratory of Advanced Technology for Materials Synthesis and Processing, Wuhan University of Technology, Wuhan 430070, China; Foshan Xianhu Laboratory of the Advanced Energy Science and Technology Guangdong Laboratory, Xianhu hydrogen Valley, Foshan 528200, China*

Jinlong Yang − *College of Materials Science and Engineering, Shenzhen University, Shenzhen 518060, China*

Jingjing Ma − *State Key Laboratory of Advanced Technology for Materials Synthesis and Processing, Wuhan University of Technology, Wuhan 430070, China*

Qian Wu − *State Key Laboratory of Advanced Technology for Materials Synthesis and Processing, Wuhan University of Technology, Wuhan 430070, China*

Wei Qian − *Hubei Engineering Research Center of RF-Microwave Technology and Application, Wuhan University of Technology, Wuhan 430070, China*

Zhe Wang − *Hubei Engineering Research Center of RF-Microwave Technology and Application, Wuhan University of Technology, Wuhan 430070, China*

Haining Zhang − *State Key Laboratory of Advanced Technology for Materials Synthesis and Processing, Wuhan University of Technology, Wuhan 430070, China;* orcid.org/0000-0002-5546-2347

Complete contact information is available at: https://pubs.acs.org/10.1021/acssuschemeng.1c02414

Author Contributions

⊥Y.Z. and J.Y. made equal contributions.

Notes

The authors declare no competing financial interest.

ACKNOWLEDGMENTS

This work was supported by the National Key Research and Development Program of China (No. 2016YFA0202603), the National Natural Science Foundation of China (51701146, 22075223), the 2018 National Key R&D Program of China (257), and the Fundamental Research Funds for the Central Universities (WUT: 2020IB005).

REFERENCES

(1) Goodenough, J. B.; Kim, Y. Challenges for Rechargeable Li Batteries. *Chem. Mater.* **2010**, *22*, 587−603.

(2) Kang, N.; Lin, Y.; Yang, L.; Lu, D.; Xiao, J.; Qi, Y.; Cai, M. Cathode porosity is a missing key parameter to optimize lithium-sulfur battery energy density. *Nat. Commun.* **2019**, *10*, 4597.

(3) Li, P.; Hwang, J.; Sun, Y. Nano/Microstructured Silicon-Graphite Composite Anode for High-Energy-Density Li-Ion Battery. *ACS Nano* **2019**, *13*, 2624−2633.

(4) Yu, F.; Que, L.; Xu, C.; Wang, M.; Sun, G.; Duh, J.; Wang, Z. Dual conductive surface engineering of Li-Rich oxides cathode for superior high-energy-density Li-Ion batteries. *Nano Energy* **2019**, *59*, 527−536.

(5) Bao, L.; Yao, J.; Zhao, S.; Lu, Y.; Su, Y.; Chen, L.; Zhao, C.; Wu, F. Densely Packed 3D Corrugated Papery Electrodes as Polysulfide Reservoirs for Lithium-Sulfur Battery with Ultrahigh Volumetric Capacity. *ACS Sustainable Chem. Eng.* **2020**, *8*, 5648−5661.

(6) Liu, P.; Wang, Y.; Hao, H.; Basu, S.; Feng, X.; Xu, Y.; Boscoboinik, J. A.; Nanda, J.; Watt, J.; Mitlin, D. Stable Potassium Metal Anodes with an All-Aluminum Current Collector through Improved Electrolyte Wetting. *Adv. Mater.* **2020**, *32*, 2002908.

(7) Wu, Q.; Yang, J.; Zhao, Y.; Song, R.; Wang, Z.; Huang, Z.; Shi, M.; Ye, Y.; He, D.; Mu, S. Lifting the energy density of lithium ion batteries using graphite film current collectors. *J. Power Sources* **2020**, *455*, 227991.

(8) Lu, H.; Hagberg, J.; Lindbergh, G.; Cornell, A. Li4Ti5O12 flexible, lightweight electrodes based on cellulose nanofibrils as binder and carbon fibers as current collectors for Li-ion batteries. *Nano Energy* **2017**, *39*, 140−150.

(9) Myung, S.; Hitoshi, Y.; Sun, Y. Electrochemical behavior and passivation of current collectors in lithium-ion batteries. *J. Mater. Chem.* **2011**, *21*, 9891−9911.

(10) Zhang, C.; Lyu, R.; Lv, W.; Li, H.; Jiang, W.; Li, J.; Gu, S.; Zhou, G.; Huang, Z.; Zhang, Y.; Wu, J.; Yang, Q. H.; Kang, F. A Lightweight 3D Cu Nanowire Network with Phosphidation Gradient as Current Collector for High-Density Nucleation and Stable Deposition of Lithium. *Adv. Mater.* **2019**, *31*, 1904991.

(11) Wang, K.; Luo, S.; Wu, Y.; He, X.; Zhao, F.; Wang, J.; Jiang, K.; Fan, S. Super-Aligned Carbon Nanotube Films as Current Collectors for Lightweight and Flexible Lithium Ion Batteries. *Adv. Funct. Mater.* **2013**, *23*, 846−853.

(12) Yi, Z.; Lin, N.; Zhao, Y.; Wang, W.; Qian, Y.; Zhu, Y.; Qian, Y. A flexible micro/nanostructured Si microsphere cross-linked by

highly-elastic carbon nanotubes toward enhanced lithium ion battery anodes. *Energy Storage Materials* **2019**, *17*, 93−100.
(13) Yuan, W.; Pan, B.; Qiu, Z.; Peng, Z.; Ye, Y.; Huang, Y.; Huang, H.; Tang, Y. Using Orthogonal Ploughing/Extrusion to Fabricate Three-Dimensional On-Chip-Structured Current Collector for Lithium-Ion Batteries. *ACS Sustainable Chem. Eng.* **2019**, *7*, 12910−12919.
(14) Chung, S.; Manthiram, A. Low-cost, porous carbon current collector with high sulfur loading for lithium-sulfur batteries. *Electrochem. Commun.* **2014**, *38*, 91−95.
(15) Bo, Z.; Zhu, W.; Ma, W.; Wen, Z.; Shuai, X.; Chen, J.; Yan, J.; Wang, Z.; Cen, K.; Feng, X. Vertically Oriented Graphene Bridging Active-Layer/Current-Collector Interface for Ultrahigh Rate Supercapacitors. *Adv. Mater.* **2013**, *25*, 5799−5806.
(16) Richard Prabakar, S. J.; Hwang, Y.; Bae, E. G.; Lee, D. K.; Pyo, M. Graphene oxide as a corrosion inhibitor for the aluminum current collector in lithium ion batteries. *Carbon* **2013**, *52*, 128−136.
(17) Lin, L.; Peng, H.; Liu, Z. Synthesis challenges for graphene industry. *Nat. Mater.* **2019**, *18*, 520−524.
(18) Fang, B.; Chang, D.; Xu, Z.; Gao, C. A Review on Graphene Fibers: Expectations, Advances, and Prospects. *Adv. Mater.* **2020**, *32*, 1902664.
(19) Guo, W.; Yu, C.; Li, S.; Yang, J.; Liu, Z.; Zhao, C.; Huang, H.; Zhang, M.; Han, X.; Niu, Y.; Qiu, J. High-Stacking-Density, Superior-Roughness LDH Bridged with Vertically Aligned Graphene for High-Performance Asymmetric Supercapacitors. *Small* **2017**, *13*, 1701288.
(20) Zhu, X.; Ye, J.; Lu, Y.; Jia, X. 3D Graphene Nanostructure Composed of Porous Carbon Sheets and Interconnected Nanocages for High-Performance Lithium-Ion Battery Anodes and Lithium-Sulfur Batteries. *ACS Sustainable Chem. Eng.* **2019**, *7*, 11241−11249.
(21) Wang, M.; Tang, M.; Chen, S.; Ci, H.; Wang, K.; Shi, L.; Lin, L.; Ren, H.; Shan, J.; Gao, P.; Liu, Z.; Peng, H. Graphene-Armored Aluminum Foil with Enhanced Anticorrosion Performance as Current Collectors for Lithium-Ion Battery. *Adv. Mater.* **2017**, *29*, 1703882.
(22) Kim, S. Y.; Song, Y. I.; Wee, J.; Kim, C. H.; Ahn, B. W.; Lee, J. W.; Shu, S. J.; Terrones, M.; Kim, Y. A.; Yang, C. Few-layer graphene coated current collectors for safe and powerful lithium ion batteries. *Carbon* **2019**, *153*, 495−503.
(23) Chen, Y.; Fu, K.; Zhu, S.; Luo, W.; Wang, Y.; Li, Y.; Hitz, E.; Yao, Y.; Dai, J.; Wan, J.; Danner, V. A.; Li, T.; Hu, L. Reduced Graphene Oxide Films with Ultrahigh Conductivity as Li-Ion Battery Current Collectors. *Nano Lett.* **2016**, *16*, 3616−3623.
(24) Lin, D.; Liu, Y.; Liang, Z.; Lee, H.; Sun, J.; Wang, H.; Yan, K.; Xie, J.; Cui, Y. Layered reduced graphene oxide with nanoscale interlayer gaps as a stable host for lithium metal anodes. *Nat. Nanotechnol.* **2016**, *11*, 626−632.
(25) Lai, D.; Chen, X.; Wang, G.; Xu, X.; Wang, Y. Highly conductive porous graphene film with excellent folding resilience for exceptional electromagnetic interference shielding. *J. Mater. Chem. C* **2020**, *8*, 8904−8916.
(26) Wang, J.; Tan, H.; Xiao, D.; Navik, R.; Goto, M.; Zhao, Y. Preparation of waterborne graphene paste with high electrical conductivity. *Chem. Phys. Lett.* **2020**, *741*, 137098.
(27) Chen, H.; Müller, M. B.; Gilmore, K. J.; Wallace, G. G.; Li, D. Mechanically Strong, Electrically Conductive, and Biocompatible Graphene Paper. *Adv. Mater.* **2008**, *20*, 3557−3561.
(28) Lu, Y.; Yang, X.; Su, B. Self-assembly to monolayer graphene film with high electrical conductivity. *J. Energy Chem.* **2013**, *22*, 52−57.
(29) Wang, X.; Zhi, L.; Müllen, K. Transparent, Conductive Graphene Electrodes for Dye-Sensitized Solar Cells. *Nano Lett.* **2008**, *8*, 323−327.
(30) Huang, H.; Zhou, F.; Shi, X.; Qin, J.; Zhang, Z.; Bao, X.; Wu, Z. Graphene aerogel derived compact films for ultrafast and high-capacity aluminum ion batteries. *Energy Storage Materials* **2019**, *23*, 664−669.
(31) Yang, W.; Gong, Y.; Zhao, X.; Liu, T.; Zhang, Y.; Chen, F.; Fu, Q. Strong and Highly Conductive Graphene Composite Film Based on the Nanocellulose-Assisted Dispersion of Expanded Graphite and Incorporation of Poly(ethylene oxide). *ACS Sustainable Chem. Eng.* **2019**, *7*, 5045−5056.
(32) Feng, S.; Yao, T.; Lu, Y.; Hao, Z.; Lin, S. Quasi-industrially produced large-area microscale graphene flakes assembled film with extremely high thermoelectric power factor. *Nano Energy* **2019**, *58*, 63−68.
(33) Liu, Y.; Zeng, J.; Han, D.; Wu, K.; Yu, B.; Chai, S.; Chen, F.; Fu, Q. Graphene enhanced flexible expanded graphite film with high electric, thermal conductivities and EMI shielding at low content. *Carbon* **2018**, *133*, 435−445.
(34) Wang, M.; Yang, H.; Wang, K.; Chen, S.; Ci, H.; Shi, L.; Shan, J.; Xu, S.; Wu, Q.; Wang, C.; Tang, M.; Gao, P.; Liu, Z.; Peng, H. Quantitative Analyses of the Interfacial Properties of Current Collectors at the Mesoscopic Level in Lithium Ion Batteries by Using Hierarchical Graphene. *Nano Lett.* **2020**, *20*, 2175−2182.
(35) Tsuchiya, Y.; Yoshiki, M.; Koga, J.; Nishiyama, A.; Koyama, M.; Ogawa, M.; Zaima, S. Effective Work Function Control With Aluminum Postdoping in the Ni Silicide/HfSiON Systems. *IEEE Trans. Electron Devices* **2008**, *55*, 2648−2656.
(36) Liu, P.; Wei, Y.; Jiang, K.; Sun, Q.; Zhang, X.; Fan, S.; Zhang, S.; Ning, C.; Deng, J. Thermionic emission and work function of multiwalled carbon nanotube yarns. *Phys. Rev. B: Condens. Matter Mater. Phys.* **2006**, *73*, 235412.
(37) Tong, L.; Wang, P.; Chen, A.; Qiu, F.; Fang, W.; Yang, J.; Wang, C.; Yang, Y. Improved electrochemical performance of binder-free multi-layered silicon/carbon thin film electrode for lithium-ion batteries. *Carbon* **2019**, *153*, 592−601.

https://doi.org/10.1021/acssuschemeng.1c02414
ACS Sustainable Chem. Eng. 2021, 9, 8635−8641